JACS
JOURNAL OF THE AMERICAN CHEMICAL SOCIETY
Article
pubs.acs.org/JACS

Unraveling the Photoluminescence Response of Light-Switching Ruthenium(II) Complexes Bound to Amyloid-β

Nathan P. Cook,[†] Mehmet Ozbil,[∥] Christina Katsampes,[†] Rajeev Prabhakar,*[,∥] and Angel A. Martí*[,†,‡,§]

[†]Department of Chemistry, [‡]Department of Bioengineering, and [§]Institute of Biosciences and Bioengineering, Rice University, Houston, Texas 77005, United States

[∥]Department of Chemistry, University of Miami, Coral Gables, Florida 33146, United States

Supporting Information

ABSTRACT: Photoluminescent molecules are widely used for real-time monitoring of peptide aggregation. In this Article, we detail both experimental and computational modeling to elucidate the interaction between $[Ru(bpy)_2dppz]^{2+}$ and amyloid-β ($A\beta_{1-40}$) aggregates. The transition from monomeric to fibrillar Aβ is of interest in the study of Alzheimer's disease. Concentration-dependent experiments allowed the determination of a dissociation constant of 2.1 μM, while Job plots provided a binding stoichiometry of 2.6 Aβ monomers per $[Ru(bpy)_2dppz]^{2+}$. Our computational approach that combines molecular docking (both rigid and flexible) and all-atom molecular dynamics (MD) simulations predicts that the hydrophobic cleft between Val18 and Phe20 is a plausible binding site, which could also explain the increase in photoluminescence of $[Ru(bpy)_2dppz]^{2+}$ upon binding. This binding site is parallel to the fibril axis, in marked contrast to the binding site of these complexes in DNA (perpendicular to the DNA axis). Other binding sites may exist at the edges of the Aβ fibril, but they are actually of low abundance in an Aβ fibril several micrometers long. The assignment of the binding site was confirmed by binding studies in an Aβ fragment ($A\beta_{25-35}$) that lacked the amino acids necessary to form the binding site. The agreement between the experimental and computational work is remarkable and provides a general model that can be used for studying the interaction of amyloid-binding molecules to Aβ.

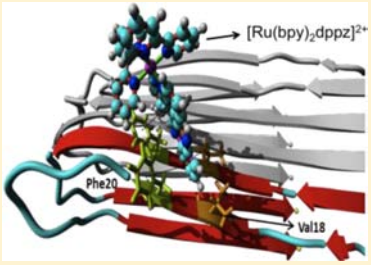

INTRODUCTION

Amyloid-β (Aβ) is a 39−43 amino acid-containing byproduct of the amyloid precursor protein (APP) and is thought to play a causative role in the progression of Alzheimer's disease (AD).[1] The amyloid cascade hypothesis suggests that the transition of monomeric Aβ into higher order aggregates is a driving factor in the progression of AD.[2] Additionally, recent studies have revealed that Aβ fibrils can template the formation of neurotoxic Aβ oligomers.[3] Molecules capable of binding on the surface of Aβ fibrils might be able to obstruct the access of Aβ monomers to its surface, inhibiting the templated formation of Aβ oligomeric species. The discovery that ruthenium dipyridophenazine complexes can bind to Aβ fibrils displaying a marked increase in photoluminescence intensity is relevant and timely,[4] because contrary to most dyes for Aβ detection, these ruthenium dyes are not planar and are easily modifiable. These characteristics, combined with their ability to bind to Aβ, make them potential parent complexes for the production of compounds capable of inhibiting Aβ aggregation or to quench the production of toxic Aβ oligomeric species induced by Aβ fibrils. Nonetheless, this will require a profound understanding of the interactions of ruthenium dipyridophenazine complexes and Aβ.

It is important to recognize that one of the main challenges of identifying binding sites on Aβ is the absence of high-resolution crystalline structures of the Aβ aggregates, which makes understanding the action of small molecule binding to the Aβ peptide difficult. Recently, structural models of Aβ have been developed with help from NMR spectroscopy.[5−7] These models have been used in combination with computational methods to examine the physical basis for probe binding,[8−11] analysis of potential inhibitors,[12−16] and structural characteristics of the aggregates and prefibrillar forms.[17]

The role of computer simulations regarding the aggregation of Aβ was recently reviewed by Lemkul and Bevan.[18] These simulations have helped elucidate probe−peptide complexes by identifying key residues and forces that foster these specific interactions.[8,10,11] Computational methods have been widely used for studying the binding modes and interactions of dyes such as Thioflavin-T (ThT)[9,19] and Congo Red (CR)[10,11] toward Aβ. Furthermore, a recent publication by one of our laboratories reported the computational modeling of the binding of cotinine with Aβ.[20] Given that these molecules have a special affinity for amyloid fibrils, identifying binding sites could be helpful for developing drugs to prevent or reverse peptide aggregation.[21] On the other hand, concentration-dependent biophysical studies have shed light on the stability of these interactions and the size of the binding site.[22,23]

In this Article, we combine biophysical and computational studies to elucidate the binding modes of $[Ru(bpy)_2dppz]^{2+}$ (bpy = 2,2′-bipyridine; dppz = dipyrido[3,2-*a*:2′,3′-*c*]-

Received: May 14, 2013
Published: July 11, 2013

   dx.doi.org/10.1021/ja404850u | J. Am. Chem. Soc. 2013, 135, 10810−10816

phenazine) to $A\beta_{1-40}$ fibrils. Ruthenium dipyridophenazine metal complexes have been used in a wide variety of applications including DNA detection,[24] cell viability studies,[25] solubilization of carbon nanotubes,[26] and cell imaging,[27−29] but have rarely been used for studying peptides.[30,31] Here, we report studies that have allowed us to generate a general picture to explain the interactions and light-switching behavior of $[Ru(bpy)_2dppz]^{2+}$ when in the presence of fibrillar Aβ peptides. Understanding how these metal complexes bind to fibrillar Aβ has general implications in the design of amyloid probes, as well as potential imaging and therapeutic agents for Alzheimer's disease.

EXPERIMENTAL SECTION

Preparation of Aβ. Bulk $A\beta_{1-40}$ (lot no. 9596) was purchased from 21st Century Biochemicals and purified and stored following previously reported methods.[4]

Preparation of Fibrillar Aggregates. Aβ fibrils were formed from a purified lyophilized powder by reconstituting the peptide in a minimal amount of NaOH (2 mM NaOH adjusted to pH 10 with 100 mM NaOH).[32] The dissolved peptide was then placed in a bath sonicator for 2 min and filtered through 0.2 μm centrifuge filters (VWR). After centrifugation, the Aβ solution was diluted with PBS (100 mM phosphate buffer, 300 mM NaCl, pH 7.4) to an approximate volume of 600 μL, and the concentration was verified with an absorption coefficient of 1280 M^{-1} cm^{-1} at 280 nm using a Shimadzu 2450 UV−vis spectrophotometer. A typical initial concentration was between 150 and 170 μM. The Aβ solutions were incubated on a Boekel orbital shaker at 37 °C and 700 rpm for 24 h.

$A\beta_{25-35}$ was purchased from 21st Century Biochemicals. Each fibril sample was prepared from a 1 mg/mL sample initially dissolved in a small amount of DMSO and then diluted to 1 mL with PBS buffer as referenced above. Samples were placed in a Boekel orbital shaker and incubated at 37 °C and 400 rpm for 24 h. The photoluminescent experiments were performed by diluting $A\beta_{25-35}$ and $A\beta_{1-40}$ to 50 μM with 5 μM $[Ru(bpy)_2dppz]^{2+}$ or 5 μM ThT. Transmission electron microscope (TEM) images were prepared by drop casting the fibril solutions on glow discharged 200 mesh carbon type B coated copper grids (Ted Pella 01811) with 3% uranyl acetate applied as a negative stain. Samples were subsequently imaged on a JEOL 1230 High Contrast TEM operating at 80 kV.

Synthesis of $[Ru(bpy)_2dppz]^{2+}$. $[Ru(bpy)_2dppz]^{2+}$ *cis*-$Ru(bpy)_2Cl_2$ was used as starting reagent (Strem Chemicals), and the dppz ligand was synthesized following previous methods.[33,34] The dppz ligand and *cis*-$Ru(bpy)_2Cl_2$ were refluxed in 1:1 methanol and water with vigorous stirring for 3 h, as described by Amouyal et al.[33] After 3 h, the solution was concentrated under reduced pressure, and upon the addition of ammonium hexafluorophosphate, orange-red crystals precipitated from solution. The crystals were purified by column chromatography (4:1 dichloromethane and acetonitrile) on SiliaFlash P60 silica gel from SiliCycle. The PF_6^- salt was used for all binding experiments. Concentrated stock solutions were prepared in acetonitrile and verified with an absorption coefficient of 16 300 M^{-1} cm^{-1} at 457 nm.[35]

Photoluminescence Experiments. All steady-state photoluminescence experiments were taken on a Horiba-Jobin Yvon Fluorolog 3. $[Ru(bpy)_2dppz]^{2+}$ was excited at 440 nm, and right angle emission was obtained from 550 to 700 nm with 2 nm slit widths. Both emission and excitation were corrected for instrument dependent effects. Intensity at 640 nm was used for subsequent calculations. At high concentrations of metal complex, corrections for inner filter effects were required. This was performed following the methods of Kubista et al.[36] The photoluminescent intensity was corrected by the inner filter effect using:

$$I_{em}^{corr} = I_{em}^{obs} 10^{-A(\lambda_{ex})l_p} \quad (1)$$

where $I_{em}{}^{corr}$ is the corrected emission, $I_{em}{}^{obs}$ is the emission obtained from the spectrometer, $A(\lambda_{ex})$ is the absorbance at the excitation wavelength, and l_p is a correction factor. The correction factor l_p is given by:

$$I_{em}^{obs} = \kappa A(\lambda_{ex}) 10^{-A(\lambda_{ex})l_p} \quad (2)$$

where κ is a proportionality constant that contains instrument parameters as well as the quantum yield of the metal complex. l_p was calculated to be 0.179 by fitting Figure S1 to:

$$\log \frac{A(\lambda_{ex})}{I_{em}^{obs}} = l_p A(\lambda_{ex}) - \log \kappa \quad (3)$$

Binding Analysis. Once fibrillar Aβ content was determined, aliquots of Aβ were diluted into metal complex samples in 20 mM phosphate buffer, 0.01% NaN_3, pH 7.4, and their photoluminescence was determined. Photoluminescence intensities were corrected for inner filter effects. The dissociation constant was determined using the equation:[37]

$$PL = f_{Ru} Ru_{tot} + \frac{f_{A\beta\text{-}Ru} - f_{Ru}}{2}(Ru_{tot} + A\beta_{tot} + K_d - \sqrt{(Ru_{tot} + A\beta_{tot} + K_d)^2 - 4Ru_{tot}A\beta_{tot}}) \quad (4)$$

where PL is the photoluminescence of the $[Ru(bpy)_2dppz]^{2+}$ at different concentrations of fibrillar Aβ, f_{Ru} is a proportionality constant that correlates $[Ru(bpy)_2dppz]^{2+}$ concentration with its photoluminescence intensity, $f_{A\beta\text{-}Ru}$ is a proportionality constant that correlates the concentration of the Aβ-$[Ru(bpy)_2dppz]^{2+}$ complex with its photoluminescence intensity, $A\beta_{tot}$ is the sum of the concentration of the Aβ-$[Ru(bpy)_2dppz]^{2+}$ complex plus free Aβ, Ru_{tot} is the sum of the concentration of the Aβ-$[Ru(bpy)_2dppz]^{2+}$ complex plus free $[Ru(bpy)_2dppz]^{2+}$, and K_d is the dissociation constant. The reported K_d is an average of five independent experiments with the error calculated from student's *t* test at 80% confidence interval.

Job Plot Analysis.[38] Fibrils (prepared as previously described) were centrifuged for 30 min at 16 000*g*, and the supernatant was analyzed by UV−vis absorption to obtain the concentration of nonfibrillar Aβ, which was determined to be around 5% of the original concentration. After taking into account nonfibrillized Aβ and solvent loss due to evaporation, the Aβ fibrils were diluted to a final concentration of either 20, 50, or 100 μM. Photoluminescence was obtained by varying the metal complex−peptide ratio with fixed total concentrations ($[Ru(bpy)_2dppz]^{2+}$ + Aβ) of 20, 50, or 100 μM. The molar ratio of $[Ru(bpy)_2dppz]^{2+}$ is defined as the moles of $[Ru(bpy)_2dppz]^{2+}$ divided by the total moles in the solution, that is, $[Ru(bpy)_2dppz]^{2+}$ + Aβ. The photoluminescence intensities were corrected as described in the preceding section. The molar ratio of Aβ for any point in Figure 1b can be obtained by subtracting the molar ratio of $[Ru(bpy)_2dppz]^{2+}$ from 1. The number of Aβ monomers per ruthenium complex is calculated by dividing the molar ratio of Aβ by the molar ratio of $[Ru(bpy)_2dppz]^{2+}$ obtained from the maximum of Figure 1b.

Computational Methods. All three molecular docking procedures were performed using the Autodock Vina 1.1.2 software[39] on $A\beta_{1-40}$ fibril structures generously provided by Robert Tycko.[5] For the docking simulations, the Ru^{2+} atom is replaced by Fe^{2+} atom as the parameters for the Ru atom are not available in the program. It is a valid approximation, because the $[Ru(bpy)_2dppz]^{2+}$ complex interacts with fibrils only through its aromatic ligands. Moreover, the Fe^{2+} and Ru^{2+} atoms are similar as they are in the same group of the periodic table. To treat the complex as a whole by the Autodock Vina program, the coordination between the metal and ligands is defined as a single bond by modifying the structure in the YASARA software.[40] The size of the grid was chosen to occupy the whole ligand−peptide complex, and the spacing was kept to 1.00 Å that is a standard value for Autodock Vina. Each docking trial produced 20 poses with the exhaustiveness value of 20. In the rigid docking, the flexibility of the receptor (the Aβ fibril), was elusive. To investigate the effect of the Aβ fibril flexibility on the docked structures, the following two methods

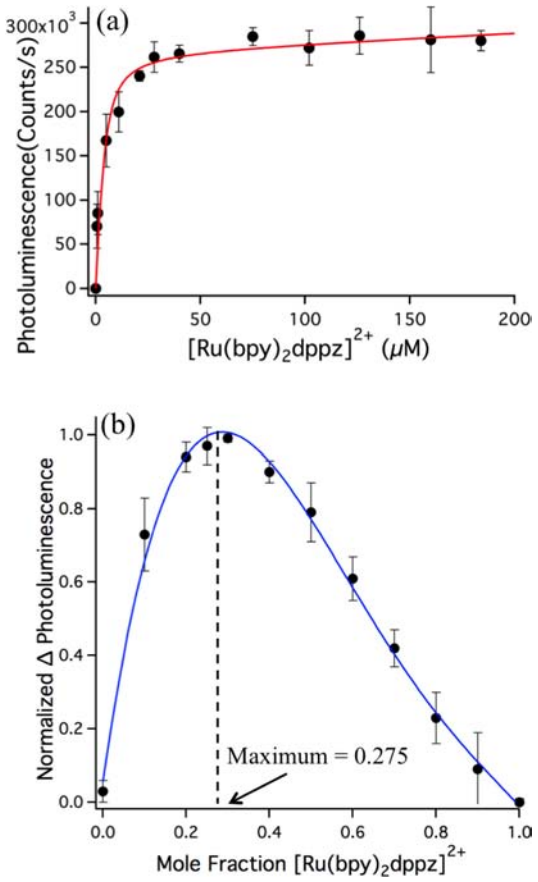

Figure 1. Binding of $[Ru(bpy)_2dppz]^{2+}$ to fibrillar Aβ. (a) Change in photoluminescence as a function $[Ru(bpy)_2dppz]^{2+}$ concentration. The concentration of Aβ was kept constant at 4 μM. The dissociation constant reported in the text is calculated from the fitting of these data (red line) and is the average of five independent experiments. (b) Job plot analysis of the photoluminescence of $[Ru(bpy)_2dppz]^{2+}$ in the presence of fibrillar Aβ. The mole fraction of the $[Ru(bpy)_2dppz]^{2+}$ and Aβ was varied, while the total concentration of the two components was kept constant at 100 μM. Δ Photoluminescence in the y axis represents the subtraction of the background $[Ru(bpy)_2dppz]^{2+}$ photoluminescence in buffer alone from the $[Ru(bpy)_2dppz]^{2+}$ photoluminescence in the presence of fibrillar Aβ. The blue curve is a polynomial fit to better illustrate the concave nature of the graph and its maximum.

were utilized: (1) flexible docking and (2) rigid docking on the different structures of the Aβ fibrils derived from a short-term (5 ns) MD simulations in an aqueous solution. The molecular dynamics (MD) simulation used in the latter was performed using the GROMACS program[41,42] utilizing the GROMOS force field GROMOS96 53A6.[42] For all simulations, the starting structures were placed in a truncated cubic box with dimensions of 100 × 100 × 100 Å. This dismisses unwanted effects that may arise from the applied periodic boundary conditions. The box was filled with single point charge (SPC) water molecules. Some water molecules were replaced by sodium and chloride ions to neutralize the system and to simulate an experimentally used ion concentration of 150 mM. The starting structures were subsequently energy-minimized with a steepest descent method for 3000 steps. The results of these minimizations produced the starting structures for the MD simulations. The MD simulations were then carried out with a constant number of particles (N), pressure (P), and temperature (T), that is, NPT ensemble. The SETTLE algorithm[43] was used to constrain the bond length and angle of the water molecules, while the LINCS algorithm[44] was used to constrain the bond length of the peptide. The long-range electrostatic interactions were calculated by the Particle-Mesh Ewald (PME) method.[45] A constant pressure of 1 bar was applied with a coupling constant of 1.0 ps; peptide, water molecules, and ions were coupled separately to a bath at 300 K with a coupling constant of 0.1 ps. The equation of motion was integrated at each 2 fs time steps. The tools available in the GROMACS program package and the YASARA program[46] have been used for analyzing trajectories and simulated structures.

The MD simulations of $[Ru(bpy)_2dppz]^{2+}$ bound to the Aβ peptide were performed using AMBER 03 force field[47] as implemented in the YASARA program[40,46] in explicit aqueous solution. The box was filled with single point charge (SPC) water molecules. The sodium and chloride ions were also added to simulate the ion concentration of 150 mM under physiological conditions. The docked poses provided in the previous step were used as the starting structures and placed into a cubic box with dimensions of 101 × 84 × 78 Å. The remaining parameters used in the simulations have been described above. Analysis of the trajectories and simulated structures were performed with the in-built tools of YASARA program. During these MD simulations C′, Cα atoms of terminal residues and atoms forming peptide bonds between residues Gln15-Lys16, Val24-Gly25, Lys28-Gly29, and Leu34-Met35 were fixed to maintain the secondary structures of $A\beta_{1-40}$ fibrils. These residues were selected due to their positions in the fibrils. The Val24-Gly25 residues are located at the end of the first β sheet, Lys28-Gly29 at the beginning of the second β sheet, and Gln15-Lys16 and Leu34-Met35 constitute two mid β sheet residue pairs. These atomic constraints help to maintain the secondary structure of fibrils without affecting the flexibility of the binding sites.

RESULTS AND DISCUSSION

As a first step, we studied the photoluminescence of $[Ru(bpy)_2dppz]^{2+}$ as a function of the concentration of fibrillized $A\beta_{1-40}$ to gain information about the $[Ru(bpy)_2dppz]^{2+}$ binding site and to assess the stability of the Aβ-$[Ru(bpy)_2dppz]^{2+}$ complex. Figure 1a shows a standard saturation curve, which can be fitted to a single-binding site with an equilibrium dissociation constant (K_d) of 2.1 ± 0.5 μM (binding constant, K_b, of 4.8 × 10^5 M^{-1}). This value is smaller than the binding constant reported for $[Ru(bpy)_2dppz]^{2+}$ bound to DNA (>10^6 M^{-1}).[48] The smaller binding constant of $[Ru(bpy)_2dppz]^{2+}$ with fibrillar Aβ implies a weaker interaction in comparison with DNA, which is consistent with the smaller increase in $[Ru(bpy)_2dppz]^{2+}$ photoluminescence with Aβ (619-fold) than with DNA (1127-fold, see Supporting Information Figure S2). The Barton group recently elucidated the X-ray structure of $[Ru(bpy)_2dppz]^{2+}$ bound to DNA and demonstrated that the dppz ligand is capable of intercalating between two well-matched stacked base pairs.[49] This intercalation provides a hydrophobic cavity that conveniently shields the dppz ligand from water. Binding sites produced by base stacking are specifically present in oligonucleotides but absent in supramolecular assemblies such as Aβ fibrils, which could explain the weaker binding interaction of $[Ru(bpy)_2dppz]^{2+}$ to Aβ aggregates. Nonetheless, the dissociation constant of $[Ru(bpy)_2dppz]^{2+}$ to fibrillar Aβ compares with the dissociation constants of ThT and CR with Aβ fibrils (0.8[23] and 1.1 μM, respectively[50]).

To further characterize the $[Ru(bpy)_2dppz]^{2+}$ binding site, we used the continuous variation method[38] to interrogate the system about the number of Aβ monomers associated with the binding of $[Ru(bpy)_2dppz]^{2+}$. The curve generated, also known as a Job plot, can be seen in Figure 1b and shows that the maximum of the $[Ru(bpy)_2dppz]^{2+}$ molar fraction is between the 0.25 and the 0.30 values. Therefore, we have decided to use these values as the uncertainty range and taken the 0.275 middle value as the curve maximum. This allows determining a

dx.doi.org/10.1021/ja404850u | J. Am. Chem. Soc. 2013, 135, 10810−10816

binding stoichiometry of ca. 2.6 ± 0.4 Aβ monomers per every $[Ru(bpy)_2dppz]^{2+}$ bound to the fibril. Job plots generated using total concentrations (Aβ+$[Ru(bpy)_2dppz]^{2+}$) of 100, 50, and 20 μM are indistinguishable from one another (see Supporting Information, Figure S3). Previous studies for ThT have identified 6.3 Aβ monomers per bound ThT,[23] and 1.7 per bound CR.[50] The binding stoichiometry of $[Ru(bpy)_2dppz]^{2+}$ and ThT tends to indicate that multiple Aβ monomers need to come together to form a binding site. This is consistent with the strong photoluminescence of $[Ru(bpy)_2dppz]^{2+}$ in the presence of Aβ fibrils but not when in contact with monomers. The smaller binding stoichiometry for CR could be attributed to the association of multiple CR molecules to the same binding site,[10] or to the availability of multiple binding sites.[11] It is important to point out that the maximum of the curve in Figure 1b is not sharp but rather broad, which suggests that there could be some slight variation in the binding stoichiometry. This is rather expected because, contrary to enzymes, which have well-defined active sites that match the shape of the target molecule, the binding site of Aβ fibrils will likely allow the $[Ru(bpy)_2dppz]^{2+}$ to assume slightly different conformations, resulting in a small continuum of binding stoichiometries.

The identification of the exact binding sites between $[Ru(bpy)_2dppz]^{2+}$ and Aβ_{1-40} fibril would require a high-resolution structure of the Aβ-$[Ru(bpy)_2dppz]^{2+}$ complex, which is challenging to obtain by either NMR or X-ray diffraction. To overcome this, we have utilized three different molecular docking techniques and MD simulations. In the past few years, computational approaches have emerged as a powerful tool for studying protein−ligand interactions. Here, the binding of $[Ru(bpy)_2dppz]^{2+}$ to Aβ_{1-40} fibril models with either two-fold[5] or three-fold[7] symmetry was investigated using (1) rigid docking, (2) flexible docking, and (3) rigid docking on different conformations of fibrils derived from short-term MD simulations. The last two approaches include flexibility of the receptor, and the details of all of these procedures are provided in the Supporting Information. The results were similar using the three methods and are summarized in Figure 2 for fibrils with two-fold symmetry,[5] which are likely the most abundant Aβ polymorph in the sample.[51] For two-fold symmetry Aβ fibril, four major sites were found, with occupation percentages of A = 46.9%, B = 16.2%, C = 15.6%, and D = 13.8%. Although four different binding sites were located, it is noteworthy that sites A and B are located at the ends of the fibril (Figure 2a). Binding sites at the end of the fibrils are scarce given the fibrillar elongation displayed by Aβ, and therefore their contribution to the binding of $[Ru(bpy)_2dppz]^{2+}$ is negligible. For example, a fibril several micrometers long with thousands Aβ monomers will have a maximum of 4 A sites and 4 B sites. In contrast to this, sites C and D run longitudinally to the fibril axis, and their number would increase as more monomers are added and the fibril is elongated. Therefore, it is plausible that sites C and D (Figure 2b) are mostly responsible for the binding of $[Ru(bpy)_2dppz]^{2+}$ to Aβ_{1-40} fibrils. A more detailed discussion about the binding sites of $[Ru(bpy)_2dppz]^{2+}$ to Aβ_{1-40} fibrils can be found in the Supporting Information.

A reliable model for the binding of $[Ru(bpy)_2dppz]^{2+}$ to Aβ should be consistent with both biophysical and computational data; however, a few inconsistencies can be found when both sets of data are compared. Especially, the data in Figure 1a fit well to a single site model in contrast with the two sites (sites C and D) found in the molecular docking experiments. Second,

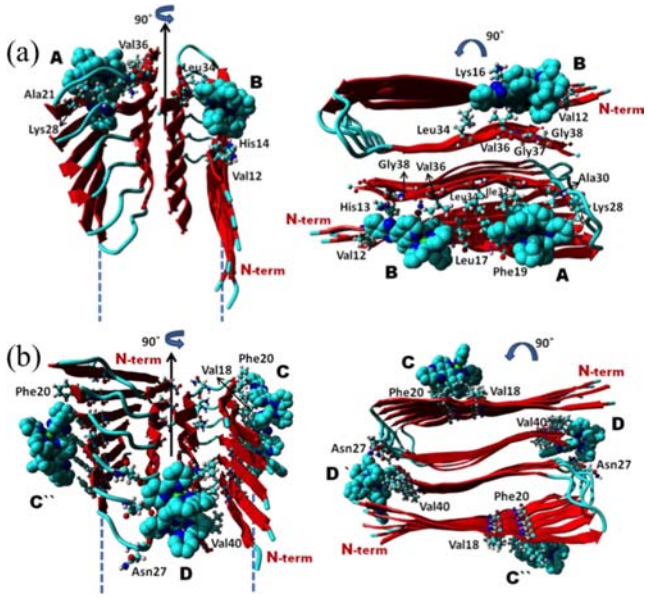

Figure 2. Binding modes of $[Ru(bpy)_2dppz]^{2+}$ on Aβ fibrils. (a) Binding sites in fibril edges (sites A and B) observed perpendicular (left) and through (right) to the fibril axis. (b) Binding sites along the fibril axis (sites C and D) observed perpendicular (left) and through (right) the fibril axis. Circular arrow indicates the position of the 2-fold rotational axis.

the Job plot in Figure 1b suggests also a single binding stoichiometry with ca. 2.6 Aβ monomers per $[Ru(bpy)_2dppz]^{2+}$. To account for these observations, we propose that site C is mainly responsible for the binding with only marginal binding to site D. The two-fold symmetry representation used to model the interactions of $[Ru(bpy)_2dppz]^{2+}$ with Aβ fibrils only contains amino acids from positions 9−40, which are the ones that form the fibril backbone. Amino acids 1−8 are in a random coil conformation, occupying most of the region where site D is found. This should block the access of $[Ru(bpy)_2dppz]^{2+}$ to site D and dramatically reduce its binding. In contrast, site C is right at the surface of the fibril and accessible for $[Ru(bpy)_2dppz]^{2+}$ binding. Furthermore, molecular modeling shows that even without this random coil region, the binding energy of site C (−9.1 kcal/mol) is more negative than that of site D (−8.7 kcal/mol), and the percentage of $[Ru(bpy)_2dppz]^{2+}$ bound to site C (15.6%) is larger than that to site D (13.8%).[52]

We have also investigated the stability of site C using 10 ns all-atom classical molecular dynamics (MD) simulations in explicit aqueous solution. These simulations were performed using AMBER force field as implemented in the YASARA program.[47] The $[Ru(bpy)_2dppz]^{2+}$ complex on the Aβ_{1-40} fibrils was found to remain intact throughout the simulations. However, a slight change in the orientation of the complex was observed. The $Ru(bpy)_2$ part of the complex raises slightly from the fibril axis in comparison with the previous buried position obtained by molecular docking (Figure 3, and Supporting Information Figure S6). In the new position, due to a better alignment of two aromatic rings of Phe20 of the fibrils and the dppz ring of the metal complex, the $\pi-\pi$ interactions between them become stronger, while the number of CH$-\pi$ interactions between the side chain of Val18 and dppz ring of the complex decreases (Supporting Information Figure S7).

dx.doi.org/10.1021/ja404850u | J. Am. Chem. Soc. 2013, 135, 10810−10816

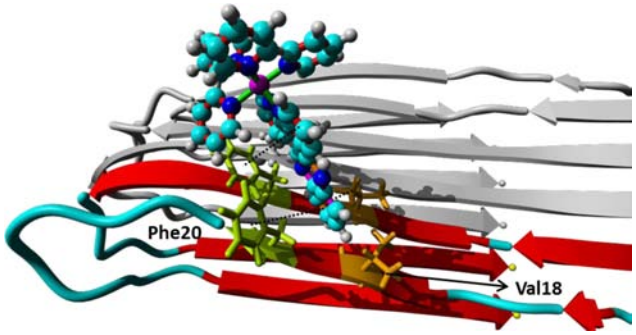

Figure 3. Binding of $[Ru(bpy)_2dppz]^{2+}$ to Aβ by MD simulation. The binding site is formed between Val18 and Phe20 (previously identified as site C). The red-marked peptides represent the projection of the $[Ru(bpy)_2dppz]^{2+}$ complex on the Aβ axis. This represents ca. 2 Aβ monomers per $[Ru(bpy)_2dppz]^{2+}$.

The assignment of site C as the dominating binding site of $[Ru(bpy)_2dppz]^{2+}$ to Aβ is consistent with the biophysical experiments. The value of 2.6 Aβ monomers per $[Ru(bpy)_2dppz]^{2+}$ determined using the Job plot in Figure 1b is in agreement with the 2.0 monomers per ruthenium complex obtained from MD simulations (Figure 3), as well as the single binding site obtained from Figure 1a. The slightly smaller value calculated from MD simulation is expected because it considers the minimum space that the complex could possibly occupy. In reality, the distance between adjacent complexes is expected to be larger to minimize electrostatic repulsion and steric constrains. Site C is a hydrophobic cleft formed between Val18 and Phe20. At this site, the side chains of Val18 and Phe20 interact with the aromatic ring of dppz through CH$-\pi$ and $\pi-\pi$ interactions, respectively (Supporting Information Figure S6). The dppz ligand is a hydrophobic extended aromatic system, which can efficiently hide from water by binding to hydrophobic domains. From Figure 3, it can be seen that the hydrophobic part of $[Ru(bpy)_2dppz]^{2+}$ (the dppz ligand) is buried into the hydrophobic cleft of site C, while the ionic part $(Ru(bpy)_2)^{2+}$ fragment) is projected outward, allowing a better solvation by water molecules. Interestingly, this observation is consistent with the light-switching properties of $[Ru(bpy)_2dppz]^{2+}$. When $[Ru(bpy)_2dppz]^{2+}$ is in water, its excitation is rapidly transferred to a low-lying dark state, which does not display any photoluminescence.[53] However, when $[Ru(bpy)_2dppz]^{2+}$ is dissolved in organic solvents or intercalated within the bases of DNA, the microenvironment around the dppz ligand changes, destabilizing the dark state and promoting the population of an emissive state, which is responsible for the photoluminescence emission. The light-switching behavior of $[Ru(bpy)_2dppz]^{2+}$ in the presence of Aβ is consistent with the binding of $[Ru(bpy)_2dppz]^{2+}$ to site C, which would provide the hydrophobic microenvironment around the dppz ligand necessary to promote the population of the emissive state, and the concomitant increase in photoluminescence.

The binding site determined for $[Ru(bpy)_2dppz]^{2+}$ is in agreement with those calculated for ThT and Congo Red. Molecular modeling has identified that both ThT and Congo red bind to amyloid forming peptides, with the long molecular axis oriented parallel to the fibril axis in agreement with our docking studies. In fact, site C is similar to the binding site identified by Wu et al. for CR.[11] Furthermore, we also analyzed the binding of $[Ru(bpy)_2dppz]^{2+}$ to Aβ_{1-40} fibrils with three-fold symmetry.[7] Although this kind of fibril is expected to be in a minimum amount (if any) in our preparations, it is a good example of a different kind of Aβ_{1-40} fibril polymorph. Interestingly, the results tend to indicate that the preferred binding site would be site K (Supporting Information Figure S5), which is again the hydrophobic cleft formed between Val18 and Phe20. The stability of site K was also probed by 10 ns all-atom classical molecular dynamics (MD) simulations in explicit aqueous solution. These simulations confirmed that the complex has a preference for this Val18-Phe20 hydrophobic cleft; although similar to the fibrils with 2-fold symmetry, changes in the orientation of the complex were observed. Nonetheless, it would be reasonable to think that this hydrophobic cleft, formed by the self-assembly of several monomers to form a fibril structure, is a general biding site for $[Ru(bpy)_2dppz]^{2+}$, which will likely be found in different polymorphic conformations of Aβ fibrils.

It is important to mention that the computational simulations presented were performed using Δ-$[Ru(bpy)_2dppz]^{2+}$; however, we also investigated the binding of the Λ-$[Ru(bpy)_2dppz]^{2+}$ enantiomer. Interestingly, upon docking the isomer to sites C and D, no significant changes in the binding poses and binding frequencies were observed, which contrasts with its behavior in DNA that shows significant variations in photoluminescent intensity and lifetime depending on the bound enantiomer.[31,54] We are currently investigating the binding of the pure Δ- and Λ-$[Ru(bpy)_2dppz]^{2+}$ enantiomers to Aβ using biophysical techniques, and the results will be reported in a future publication.

So far, our experimental results have shown that $[Ru(bpy)_2dppz]^{2+}$ binds to a single binding site and that this site is formed by ca. 2.6 monomers. Our computational simulations have identified a hydrophobic cleft between Val 18 and Phe 20 as the binding site for $[Ru(bpy)_2dppz]^{2+}$. This remarkable agreement between the experimental and computational studies has led us to propose that this site formed by Val 18 and Phe 20 and that runs throughout the fibril axis is responsible for "turning on the photoluminescence switch" of $[Ru(bpy)_2dppz]^{2+}$. To further demonstrate this assignment, we have studied the binding of $[Ru(bpy)_2dppz]^{2+}$ to Aβ_{25-35}, an amyloid peptide fragment that lacks the Val18-Phe20 binding site but that forms amyloid fibrils and binds other Aβ binding dyes such as ThT (see Supporting Information Figure S8).[55,56] Figure 4 shows the photoluminescence of $[Ru(bpy)_2dppz]^{2+}$ in the presence of fibrillar Aβ_{25-35} and Aβ_{1-40}. When $[Ru(bpy)_2dppz]^{2+}$ is in contact with Aβ_{1-40} fibrils, its photoluminescence increases by more than 65-fold, while when in contact with Aβ_{25-35} fibrils, the increase in photoluminescence is small (7-fold). The low photoluminescence response indicates a poor interaction between $[Ru(bpy)_2dppz]^{2+}$ and Aβ_{25-35}, which demonstrates that the hydrophobic cleft formed by Val18 and Phe20 is of great importance for the binding and photoluminescence response of $[Ru(bpy)_2dppz]^{2+}$.

CONCLUSIONS

In summary, our binding and computational experiments have led us to conclude that $[Ru(bpy)_2dppz]^{2+}$ binds to a hydrophobic cleft, formed on the surface of Aβ fibrils between Val18 and Phe20 which is responsible for the "light-switching" properties of this ruthenium dipyridophenazine complex. The great consistency between the biophysical studies and the computational simulations found in this study validates the proposed model and offers a guide for identifying the binding

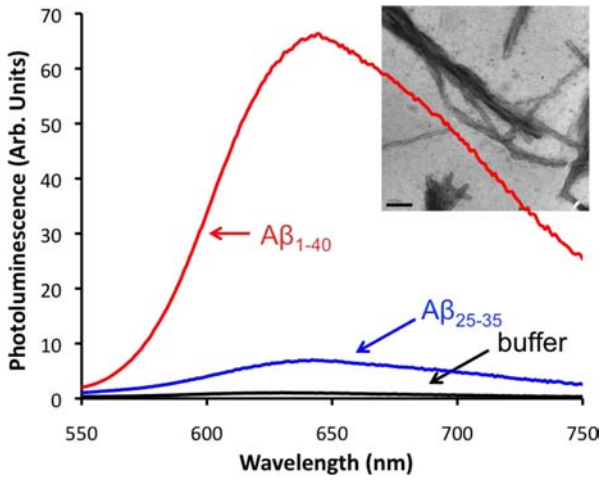

Figure 4. Photoluminescence of $[Ru(bpy)_2dppz]^{2+}$ with fibrillar Aβ. Photoluminescence spectra of $[Ru(bpy)_2dppz]^{2+}$ incubated with fibrillar Aβ_{1-40} (red line), fibrillar Aβ_{25-35} (blue line), and buffer (black line). Inset shows a TEM image of Aβ_{25-35} fibrils. Scale bar 200 nm.

sites of other amyloid binding molecules. Although other binding sites could exist, those do not cause an increase in the photoluminescence of $[Ru(bpy)_2dppz]^{2+}$ upon binding, or are too scarce to produce any measurable effect (such as terminal sites A and B). It is important to point out that $[Ru(bpy)_2dppz]^{2+}$ binds DNA with the dppz ligand perpendicular to the DNA strand axis, while the binding to Aβ is parallel to the fibril axis. This parallel binding mode is unprecedented for $[Ru(bpy)_2dppz]^{2+}$ and opens a new window of possibilities for the binding of this complex to other molecular architectures containing long hydrophobic domains on their surface. In addition, this research provides hard evidence of the ability of a hydrophobic cleft in the surface of Aβ fibrils to bind hydrophobic molecules with extended aromatic systems. Therefore, it is reasonable to think that molecules such as coumarins and rhodamines, which have extended aromatic systems, can potentially bind Aβ in a similar way. This would allow the design of a new generation of Aβ binding molecules with potential applications in sensing and inhibition of Aβ aggregation.

■ ASSOCIATED CONTENT

Ⓢ Supporting Information

Determination of the photoluminescence correction factor, photoluminescence spectra of $[Ru(bpy)_2dppz]^{2+}$ in the presence of DNA and fibrillar Aβ, Job Plot with different Aβ concentrations, expanded discussion of the computational binding results, and photoluminescence of Aβ_{25-35} with ThT. This material is available free of charge via the Internet at http://pubs.acs.org.

■ AUTHOR INFORMATION

Corresponding Author

rpr@miami.edu; amarti@rice.edu

Notes

The authors declare no competing financial interest.

■ ACKNOWLEDGMENTS

We would like to thank Robert Tycko for generously providing the atomic coordinates for the two-fold and three-fold symmetry Aβ fibril models and Kathleen Matthews for helpful discussions. This material is based upon work supported by the grants of the Welch Foundation (grant no. C-1743) to A.A.M., the National Science Foundation (grant no. 1152846), and the James and Esther King Biomedical Research Program of the Florida State Health Department (grant no. 08KN-11) to R.P.

■ REFERENCES

(1) Shoji, M.; Golde, T. E.; Ghiso, J.; Cheung, T. T.; Estus, S.; Shaffer, L. M.; Cai, X.-D.; McKay, D. M.; Tintner, R.; Frangione, B.; Younkin, S. G. *Science* **1992**, *258*, 126−129.
(2) Hardy, J. A.; Higgins, G. A. *Science* **1992**, *256*, 184−185.
(3) Cohen, S. I. A.; Linse, S.; Luheshi, L. M.; Hellstrand, E.; White, D. A.; Rajah, L.; Otzen, D. E.; Vendruscolo, M.; Dobson, C. M.; Knowles, T. P. J. *Proc. Natl. Acad. Sci. U.S.A.* **2013**, *110*, 9758−9763.
(4) Cook, N. P.; Torres, V.; Jain, D.; Martí, A. A. *J. Am. Chem. Soc.* **2011**, *133*, 11121−11123.
(5) Petkova, A. T.; Yau, W.-M.; Tycko, R. *Biochemistry* **2006**, *45*, 498−512.
(6) Lührs, T.; Ritter, C.; Adrian, M.; Riek-Loher, D.; Bohrmann, B.; Döbeli, H.; Schubert, D.; Riek, R. *Proc. Natl. Acad. Sci. U.S.A.* **2005**, *102*, 17342−17347.
(7) Paravastu, A. K.; Leapman, R. D.; Yau, W.-M.; Tycko, R. *Proc. Natl. Acad. Sci. U.S.A.* **2008**, *105*, 18349−18354.
(8) Rodríguez-Rodríguez, C.; Rimola, A.; Rodríguez-Santiago, L.; Ugliengo, P.; Álvarez-Larena, Á.; Gutierrez-de-Terán, H.; Sodupe, M.; Gonzalez-Duarte, P. *Chem. Commun.* **2010**, *46*, 1156−1158.
(9) Wu, C.; Wang, Z.; Lei, H.; Duan, Y.; Bowers, M. T.; Shea, J.-E. *J. Mol. Biol.* **2008**, *384*, 718−729.
(10) Wu, C.; Wang, Z.; Lei, H.; Zhang, W.; Duan, Y. *J. Am. Chem. Soc.* **2007**, *129*, 1225−1232.
(11) Wu, C.; Scott, J.; Shea, J.-E. *Biophys. J.* **2012**, *103*, 550−557.
(12) Bruce, N. J.; Chen, D.; Dastidar, S. G.; Marks, G. E.; Schein, C. H.; Bryce, R. A. *Peptides* **2010**, *31*, 2100−2108.
(13) Lemkul, J. A.; Bevan, D. R. *Biochemistry* **2010**, *49*, 3935−3946.
(14) Raman, E. P.; Takeda, T.; Klimov, D. K. *Biophys. J.* **2009**, *97*, 2070−2079.
(15) Liu, F.-F.; Dong, X.-Y.; He, L.; Middelberg, A. P. J.; Sun, Y. *J. Phys. Chem. B* **2011**, *115*, 11879−11887.
(16) Chen, D.; Martin, Z. S.; Soto, C.; Schein, C. H. *Biorg. Med. Chem.* **2009**, *17*, 5189−5197.
(17) Buchete, N.-V.; Tycko, R.; Hummer, G. *J. Mol. Biol.* **2005**, *353*, 804−821.
(18) Lemkul, J. A.; Bevan, D. R. *ACS Chem. Neurosci.* **2012**, *3*, 845−856.
(19) Wu, C.; Bowers, M. T.; Shea, J.-E. *Biophys. J.* **2011**, *100*, 1316−1324.
(20) Echeverria, V.; Zeitlin, R.; Burgess, S.; Patel, S.; Barman, A.; Thakur, G.; Inouye, H.; Mamcarz, M.; Wang, L.; Buckingham, S. D.; Kirschner, D. A.; Mori, T.; Leblanc, R. M.; Prabhakar, R.; Sattelle, D.; Arendash, G. W. *J. Alzheimer's Dis.* **2011**, *24*, 817−835.
(21) Landau, M.; Sawaya, M. R.; Faull, K. F.; Laganowsky, A.; Jiang, L.; Sievers, S. A.; Liu, J.; Barrio, J. R.; Eisenberg, D. *PLoS Biol.* **2011**, *9*, e1001080.
(22) Groenning, M. *J. Chem. Biol.* **2010**, *3*, 1−18.
(23) Levine, H. *Amyloid* **2005**, *12*, 5−14.
(24) Erkkila, K. E.; Odom, D. T.; Barton, J. K. *Chem. Rev.* **1999**, *99*, 2777−2796.
(25) Jiménez-Hernández, M. E.; Orellana, G.; Montero, F.; Portolés, M. T. *Photochem. Photobiol.* **2000**, *72*, 28−34.
(26) Jain, D.; Saha, A.; Martí, A. A. *Chem. Commun.* **2011**, *47*, 2246−2248.
(27) Puckett, C. A.; Barton, J. K. *Biochemistry* **2008**, *47*, 11711−11716.
(28) Puckett, C. A.; Barton, J. K. *J. Am. Chem. Soc.* **2006**, *129*, 46−47.
(29) Cook, N. P.; Kilpatrick, K.; Segatori, L.; Martí, A. A. *J. Am. Chem. Soc.* **2012**, *134*, 20776−20782.

(30) Murphy, C. J.; Nair, R. B.; Keller, C. E.; Teng, E. S.; Pollard, C. *Proc. SPIE* **1997**, *2980*, 473−478.
(31) Svensson, F. R.; Abrahamsson, M.; Strömberg, N.; Ewing, A. G.; Lincoln, P. *J. Phys. Chem. Lett.* **2011**, *2*, 397−401.
(32) Fezoui, Y.; Hartley, D. M.; Harper, J. D.; Khurana, R.; Walsh, D. M.; Condron, M. M.; Selkoe, D. J.; Lansbury, P. T.; Fink, A. L.; Teplow, D. B. *Amyloid* **2000**, *7*, 166−178.
(33) Amouyal, E.; Homsi, A.; Chambron, J.-C.; Sauvage, J.-P. *Dalton Trans.* **1990**, 1841−1845.
(34) Dickeson, J.; Summers, L. *Aust. J. Chem.* **1970**, *23*, 1023−1027.
(35) Sun, Y.; Joyce, L. E.; Dickson, N. M.; Turro, C. *Chem. Commun.* **2010**, *46*, 2426−2428.
(36) Kubista, M.; Sjöback, R.; Eriksson, S.; Albinsson, B. *Analyst* **1994**, *119*, 417−419.
(37) Celej, M. S.; Jares-Erijman, E. A.; Jovin, T. M. *Biophys. J.* **2008**, *94*, 4867−4879.
(38) Huang, C. Y. *Methods Enzymol.* **1982**, *87*, 509−525.
(39) Trott, O.; Olson, A. J. *J. Comput. Chem.* **2010**, *31*, 455−461.
(40) Krieger, E.; Koraimann, G.; Vriend, G. *Proteins: Struct., Funct., Genet.* **2002**, *47*, 393−402.
(41) Lindahl, E.; Hess, B.; van der Spoel, D. *J. Mol. Model.* **2001**, *7*, 306−317.
(42) Oostenbrink, C.; Villa, A.; Mark, A. E.; van Gunsteren, W. F. *J. Comput. Chem.* **2004**, *25*, 1656−1676.
(43) Miyamoto, S.; Kollman, P. A. *J. Comput. Chem.* **1992**, *13*, 952−462.
(44) Hess, B.; Bekker, H.; Berendsen, H. J. C.; Fraaije, J. G. E. M. *J. Comput. Chem.* **1997**, *18*, 1463−1472.
(45) Darden, T. A.; York, D.; Pedersen, L. *J. Chem. Phys.* **1993**, *98*, 10089−10092.
(46) Krieger, E.; Vriend, G. *Bioinformatics* **2002**, *18*, 315−318.
(47) Duan, Y.; Wu, C.; Chowdhury, S.; Lee, M. C.; Xiong, G.; Zhang, W.; Yang, R.; Cieplak, P.; Luo, R.; Lee, T.; Caldwell, J.; Wang, J.; Kollman, P. *J. Comput. Chem.* **2003**, *24*, 1999−2012.
(48) Friedman, A. E.; Chambron, J.-C.; Sauvage, J.-P.; Turro, N. J.; Barton, J. K. *J. Am. Chem. Soc.* **1990**, *112*, 4960−4962.
(49) Song, H.; Kaiser, J. T.; Barton, J. K. *Nat. Chem.* **2012**, *4*, 615−620.
(50) Zhen, W.; Han, H.; Anguiano, M.; Lemere, C. A.; Cho, C.-G.; Lansbury, P. T. *J. Med. Chem.* **1999**, *42*, 2805−2815.
(51) The morphology of our fibrils examined by TEM is in agreement with those identified by the Tycko group as having two-fold symmetry: Paravastu, A. K.; Leapman, R. D.; Yau, W.-M.; Tycko, R. *Proc. Natl. Acad. Sci. U.S.A.* **2008**, *105*, 18349−18354 Furthermore, it was also demostrated by Tycko's group that static incubation tends to result in three-fold symmetry fibrils, while incubation under agitation forms two-fold symmetry fibrils. Our fibrils are grown under agitation.
(52) It is important to recognize that the remaining percentage is attributed to sites A and B, but only in this short fibril are fragments made of 6 Aβ monomers. Percentage contribution in a real micrometer long fibril for sites A and B is negligible.
(53) Brennaman, M. K.; Alstrum-Acevedo, J. H.; Fleming, C. N.; Jang, P.; Meyer, T. J.; Papanikolas, J. M. *J. Am. Chem. Soc.* **2002**, *124*, 15094−15098.
(54) Andersson, J.; Fornander, L. H.; Abrahamsson, M.; Tuite, E.; Nordell, P.; Lincoln, P. *Inorg. Chem.* **2013**, *52*, 1151−1159.
(55) Kellermayer, M. S. Z.; Karsai, Á.; Benke, M.; Soós, K.; Penke, B. *Proc. Natl. Acad. Sci. U.S.A.* **2008**, *105*, 141−144.
(56) Grace, E. A.; Rabiner, C. A.; Busciglio, J. *Neuroscience* **2002**, *114*, 265−273.